Particle Size Effects on Hydro-Cyclone Performance

M. H. Shojaeefard, A.R. Noorpoor, H.Yarjiabadi, M.Habibian

Abstract: The hydrocyclone has a very important roll in industrial separation. The consideration of its behavior is very important for design. In this investigation, behavior of water flow and particles trajectory inside a hydrocyclone has been considered by means of numerical and experimental methods, and results have been compared together. To have a numerical simulation, a CFD software was used, and for modeling flow the RNG $k - e$ model applied. Finally, the effect of particle size on hydrocyclone performance has been studied. It was found that the grade efficiency and number of particle that exit from underflow of the hydrocyclone is increased when bigger particles is used.
A series of experiments has been carried out in a laboratory with a hydrocyclone. Comparison shows that, there is a good agreement between the CFD models and experimental result.

Keywords: Hydrocyclone, CFD modeling, Particle size, Discrete phase.

1. Introduction

There has been a rapid growth in the use of hydro-cyclones in the chemical, mineral, coal and powder-processing industries. The reasons for this popularity is in the design and operational simplicity, high capacity, low maintenance and operating cost and the small physical size of the device. A typical hydrocyclone consists of a cylindrical section with a central tube connected to a conical section with a discharge tube. An inlet tube is attached to the top section of the cylinder. The fluid being injected tangentially into hydrocyclone causes swirling and thus generates centrifugal force within the device. This centrifugal force field brings about a rapid classification of particulate material from the medium in which it is suspended. The flow behavior in hydrocyclone is quite complex. This complexity of flow processes has led designers to rely on empirical equations for predicting the equipment performance. These empirical relationships are derived from an analysis of experimental data and include the effect of operational and geometric variables. Different sets of experimental data lead to different equations for the same basic parameters. Empirical models correlate a classification parameter, such as the cut size, with device dimensions and slurry properties (Dahlstrom, 1949; Yoshiota and

Hotta, 1955; Fahlstrom, 1963; Agar and Herbst, 1966; Lynch and Rao, 1975; Plitt, 1976) [1-6].
However, these models suffer from the inherent deficiency as any other empirical models —the model can only be used within the extremes of vortex finder and spigot dimensions were changed the experimental data from which the model parameters were determined. In view of this shortcoming, mathematical models based on fluid mechanics are highly desirable. Computational Fluid Dynamics (CFD) is a versatile means to predict velocity profiles under a wide range of design and operating conditions. The numerical treatment Navier–Stokes equations are the backbone of any CFD technique gradually crept into the analysis of the hydrocyclone in the early 1980s. This resulted from the rapid improvement in computers and a better understanding of the numerical treatment of turbulence. Bloor and Ingham (1987) applied the Navier-Stokes equation to compute the flow field in hydrocyclones and gave an analytical solution, with overly simplifying assumptions. In the region near the central axis, the vortex conservation was applied, with inviscid and rotational flow assumptions, which yields axial and radial components. In the region along the wall, the boundary-layer approach was used to derive velocities [7].
Despite Bloor and Ingham's efforts in predicting velocity data measured by Kelsal (Kelsal, 1952, a data set often referred to in numerous publications, the lack of an adequate turbulence description led others to revise the analytical solutions as necessary) [8]. The first successful work in predicting the fluid flow in hydrocyclones is that of Pericleous and Rhodes (1986) and Pericleous et al. (1984), who used the PHOENICS computer code for the solution of the partial differential equations. Using the simple Prandtl mixing

M. H. Shojaeefard., Automotive Engineering Department, Iran Univ of Science and Tech, *mhshf@ iust.ac.ir*

A.R. Noorpoor, Chemical Engineering Department, Iran Univ of Science and Tech.

H.Yarjiabadi, Automotive Engineering Department, Iran Univ of Science and Tech.

M.Habibian, Chemical Engineering Department, Iran Univ of Science and Tech.

length model and the axisymmetry assumptions, the authors reported the velocity predictions in a 200-mm hydrocyclone [9,10]. Later, Hsieh and Rajamani (1991) numerically solved the turbulent momentum equations to obtain the velocities and compared them with the Laser Doppler Velocimetry measurements in a 75-mm hydrocyclone. This work showed that, by a simple balance of forces the particle can be traced inside the hydrocyclone, from which the entire size-classification efficiency is computed [11]. In a sequence, Monredon et al. (1990) showed that the same model is evidently applicable even if the vortex finder and spigot dimensions were changed drastically, be sides the operating conditions [12]. All of these modeling works have been confined to hydrocyclones processing slurries in the $5 - 10\%$ solids range, and have mostly be unrestricted to axisymmetric geometries (Boysan et al., 1982[13]; David Son, 1988[14]). The practical constraint in 3D simulations have been the and the total amount of CPU time that may be spent on the simulation. However, few three-dimensional simulations have been reported in recent years (Cristeaetal., 1994[15]; Slack and Wraith, 1997[16]; Hoekstraetal., 1999[17]). Most of these studies have aimed to simulate only the flow of water in a hydrocyclone; very few attempts have been made to predict the flow of solids in the separator. An attempt in this study is to predict both water and solids splits in a laboratory hydrocyclone. The model predictions were also compared with experimental results.

Finally, determining grade efficiency versus particle diameter and compare with experimental results [18-20].

2. Governing Equations
2.1. Water Flow Modeling
For a dilute fluid suspension, the incompressible Navier–Stokes equations supplemented by a suitable turbulence model are appropriate for modeling the flow in a hydrocyclone. The most popular turbulence model in use for engineering applications is the k–e model where the scalar variables k and e represent the kinetic energy of turbulence and its dissipation rate, respectively. The following equations describe the steady-state conservation of mass and momentum,

$$\nabla.(r.\vec{v}) = 0 \tag{1}$$

$$\nabla.(r.\vec{v}\,\vec{v}) = -\nabla p + \nabla(\bar{t}) + r\,\bar{g} \tag{2}$$

Where p is the static pressure, $r\,\bar{g}$ is the gravitational body force. $\bar{t}$ Is the stress tensor given by,

$$\bar{t} = m_{effective}[(\nabla.\vec{v}) - \frac{2}{3}\nabla\vec{v}\,I] \tag{3}$$

Where $\qquad m_{effective} = m + m_t$

To start with, the standard k $-e$ model was used to represent the turbulence in the equipment. The model was used to predict the water flow rates in the two outlet streams for different inlet velocities of water.

2.1.1. Turbulence Modeling
The standard k $-e$ model is a semi-empirical model based on model transport equations for the turbulent kinetic energy (k) and its dissipation rate (e), and are given by:

$$\frac{\partial}{\partial t}(pk) + \frac{\partial}{\partial x_i}(pu_i k)$$
$$= \frac{\partial}{\partial x_i}\frac{m_T}{s_K}\frac{\partial k}{\partial x_i} + G_k + G_b - pe \tag{4}$$

$$\frac{\partial}{\partial t}(pe) + \frac{\partial}{\partial x_i}(pu_i e) = \frac{\partial}{\partial x_i}\frac{m_T}{s_e}\frac{\partial e}{\partial x_i}$$
$$+ C_{13.}\frac{e}{k}(G_k + (1 - C_{3e})G_b) - C_{2e.}p.\frac{e^2}{k} \tag{5}$$

$$G_k = m_T\left[\frac{\partial u_j}{\partial x_i} + \frac{\partial u_i}{\partial x_j}\right]\frac{\partial u_j}{\partial x_i} \tag{6}$$

These equations, represent turbulent kinetic energy generated due to the mean velocity gradients, $C_{1e.}$, $C_{2e.}$ and $C_{3e.}$ are constants. The ∂_k and ∂_e are the turbulent Prandtl numbers for k and e, respectively. The ''eddy'' or turbulent viscosity, m_t defined in Esq. (2) and (3) can be computed by combining k and e as follows:

$$m_t = rC_m k^2/e \tag{7}$$

Where C_m is constant. The constants of model as $C_{1e.}$, $C_{2e.}$, $C_{3e.}$, ∂_k and ∂_e were assumed to have the following values :

$$C_{1e.} = 1.44 \quad C_{2e.} = 1.92 \quad C_m = 0.09 \quad \text{and}$$
$$\partial_k = 1.0 \quad \partial_e = 1.3$$

2.2. Discrete Phase Modeling
In this modeling technique, the second phase is introduced as a discrete phase that can be simulated in a Lagrangian frame of reference by defining the initial position, velocity and size of individual particles. This second phase consists of spherical particles dispersed in the continuous phase. The initial conditions, along with the inputs defining the physical properties of the discrete phase, are used to initiate trajectory calculations. The trajectory calculations are based on the force balance on the particle, using local continuous phase conditions as the particle moves through the

flow.The formulation is the assumption that the second phase is sufficiently dilute particle–particle interactions and the effects of the particle volume fraction on the continuous phase are negligible.

2.2.1. Particles in Turbulent Flows

The dispersion of particles due to turbulence in the fluid phase was predicted using the stochastic tracking model. The stochastic tracking (or ''random walk'') model includes the effect of instantaneous turbulent velocity fluctuations on the particle trajectories through the use of stochastic methods. The particles are assumed to have no direct impact on the generation or dissipation of turbulence in the continuous phase.

2.2.2. Equations of Motion for Particles

The trajectory of the discrete phase particle is obtained by integrating the force balance on the particle, which can be written in a Lagrangian reference frame.This force balance equates the particle inertia with the forces acting on the particle, and can be written (for the x direction in Cartesian coordinates) as:
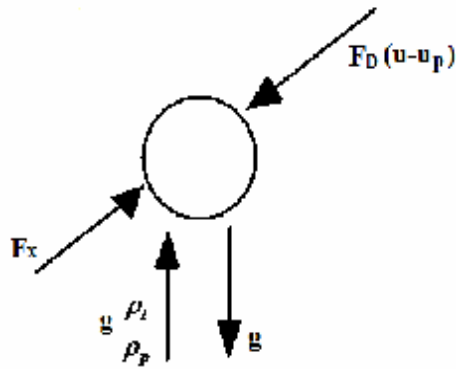
Fig. 1. Different Forces on Particle

$$\frac{Du_p}{Dt} = F_D(u - u_p) + g(\frac{r_p - r_1}{r_p}) + F_x \qquad (8)$$

Where F_x is coriolis force, $F_D(u - u_p)$ is the drag force per unit particle mass and

$$F_D = (\frac{18\,mD_p^2}{r_p})(\frac{C_D\,\text{Re}}{24}) \qquad (9)$$

Here, u is the fluid phase velocity, u_p is the particle velocity, m is the molecular viscosity of the fluid, r_1 is the fluid density, r_p is the density of the particle and D_p is the particle diameter, Re is the relative Reynolds number which is defined as

$$\text{Re} = \frac{rD_p(u_p - u)}{m} \qquad (10)$$

For sub micron particles, a form of Stroke's drag law is available and in that case F_D is defined as:

$$F_D = \frac{18m}{r_p}D_p^2 C_c \qquad (11)$$

Where

$$C_c = 1 + \left[\frac{2l}{D_p}(1.257 + 0.4\exp(-1.1(\frac{D_p}{2l}))) \right]$$

where l is the mean free path.

3. Numerical Simulation
3.1. Geometry and Grid Generation

At first, the points of shape were defined. The geometry is obtained by connecting this points.Fig.2 shows dimensions of hydrocyclone geometry and a 3-D view of hydro-cyclone are shown in Fig. 3. Fig. 4 and 5 are shown that an unstructured Tet/Hybrid mesh with 180000 elements is used for the main body of hydrocyclone. The mesh shown in Fig. 5, uses an unstructured Hex mesh for the main body of the cyclone. In strong convective flows, as in a cyclone, it is best to align the mesh to the flow direction. This prevents false diffusion (Patanker, 1980). Hexahedral mesh elements are less diffusive than other mesh element shapes such as tetrahedral. In addition to the hex elements it is preferential to use high order discretisation to further reduce the influence of false or numerical diffusion. In this example the tangential inlet shown is meshed for simplicity using tetrahedral elements. The tangential inlet is also joined to the main cyclone chamber by a small overlapping non-conformal interface.
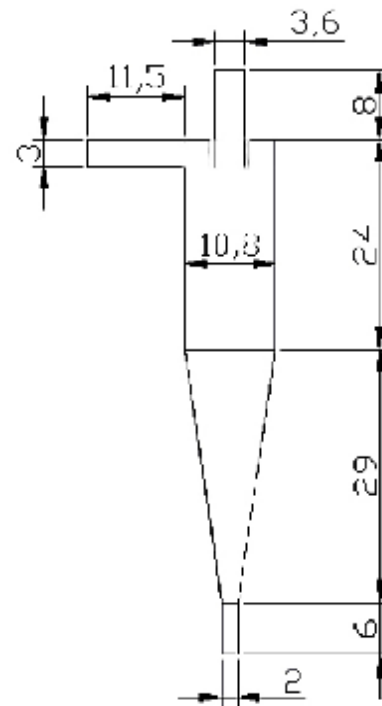

Fig. 2. Hydrocyclone Geometry Dimension (cm)

3.2. Grid Independency

The study of grid independency, how should the mesh size be varied in order to check the solution at different grid sizes to get a range at which there is no variation in the solution (Table1).
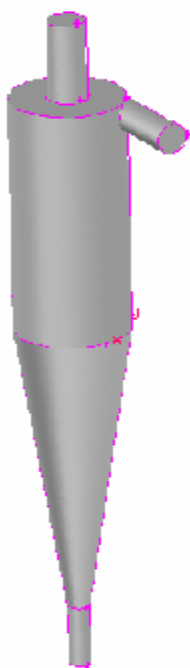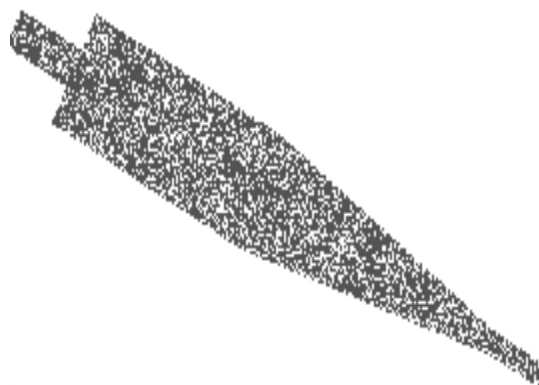
Table 1. Grid Generation Error

Number of mesh element in volume	Error in result
140000	30%
160000	16%
170000	8%
175000	7%
180000	6%
190000	6.1%

Fig. 3. 3-D View of Geometry

Fig. 4. Axial Grid of Computational Domain
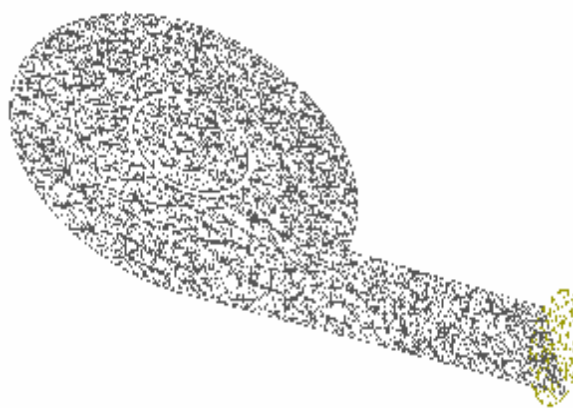
Fig. 5. Cross-Section Grid of Computational Domain

3.3. Solution

In addition to solving transport equations for the continuous phase, CFD allows to simulate a discrete second phase in a Lagrangian frame of reference.

This second phase consists of spherical particles dispersed in the continuous phase.

CFD computes the trajectories of these discrete phase entities, as well as heat and mass transfer to/from them.

The coupling between the phases and its impact on both the discrete phase trajectories and the continuous phase flow can be included.

We can include a discrete phase in our CFD model by defining the initial position, velocity, size, and temperature of individual particles.

These initial conditions, along with our inputs defining the physical properties of the discrete phase, are used to initiate trajectory and heat/mass transfer calculations.

The trajectory and heat/mass transfer calculations are based on the force balance on the particle and on the convective/radiative heat and mass transfer from the particle, using the local continuous phase conditions as the particle moves through the flow.

The predicted trajectories and the associated heat and mass transfer can be viewed graphically and/or alphanumerically.

We can use CFD to predict the discrete phase patterns based on a fixed continuous phase flow field (an uncoupled approach), or we can include the effect of the discrete phase on the continuum (a coupled approach).

In the coupled approach, the continuous phase flow pattern is impacted by the discrete phase (and vice versa), and we can alternate calculations of the continuous phase and discrete phase equations until a converged coupled solution is achieved.

3.3.1. Material Properties

The properties of fluid and particles are shown:

- *Water-liquid (fluid)*

Property	Units	Method	Value(s)
Density	kg/m³	constant	998.2
Cp (Specific Heat)	j/kg.k	constant	4182
Thermal Conductivity	w/m.k	constant	0.6
Viscosity	kg/m.s	constant	0.001
Molecular Weight	kg/kmol	constant	18.015

- *. Sand (inert-particle)*

Property	Units	Method	Value(s)
Density	kg/m³	constant	2500
Cp (Specific Heat)	j/kg.k	constant	1680
Thermal Conductivity	w/m.k	constant	0.045

3.3.2. Boundary Conditions
In Table.2 the boundary conditions for this system are shown:

Table. 2. Boundary conditions

	Water Mass (Kg/s)	Sand Mass (Kg/s)	Pressure (Pascal)
INLET	0.455	0.4	13931
OVERFLOW	Can be computed	Can be computed	0(atm)
UNDERFLOW	Can be computed	Can be computed	0(atm)

Also it is assumed that particle diameters have been 50-100 micron.

3.3.3. Operating Conditions
In this section, we define gravitational acceleration in direction y (-9.86 $\frac{m}{s^2}$) and assume operating pressure 101325 Pascal at a reference pressure location (1,1,1).

3.3.4. Solution
After defining materials, boundary conditions and operating conditions, the next step is to solve for CFD. Experience has shown that typically 6000 iterations may be needed before the peak tangential velocity in the simulation stabilizes with residuals less than 10^{-8}.

4. Results
For the conditions specified above, the results of the CFD model was compared to data obtained from a laboratory hydrocyclone with similar geometry run at the same feed density and pressure.
Table 3 shows mass flow rate in exit surfaces that compared with experience.

The contours and diagrams of quantities in hydrocyclone are shown in Fig.8- Fig.28. Fig.8 shows path lines of water in continuous phase that colored by total pressure.
This figure clearly indicates that pressure in center of surface is less than the walls.
Fig.9 clearly shows air core that colored by total pressure in a vertical face for liquid phase.
Contours of pressure and velocity in a horizontal face for water phase that satisfy no-slip condition in walls shown in Fig.10 and 11.
Fig. 12 shows path lines of particle in a readily stream line vs their pressure and Fig. 13 shows path lines of particle in a readily stream line vs their diameter.
In Fig. 14,15,16,17 contour of pressure and velocity for discrete phase are shown, that validate with experience.
Fig.18 shows line velocity in a vertical face for discrete phase. In Fig.19 vectors of velocity in a horizontal face are shown.
This figure displays that primary and secondary vortexes have same direction.
Fig.20 shows the velocity distributions at the horizontal level where the inlet pipe enters the hydrocyclone.
In Fig.21-28, plots of velocity magnitude, axial and radial velocity, static and total pressure in horizontal and vertical faces are shown.
These plots have a good agreement with experience.

Table. 3. Comparison of Experimental and CFD Modeling in Mass Flow Rate

	Water Mass (Kg/s)			Sand Mass (Kg/s)		
	Exp	CFD	Error	Exp	CFD	Error
INFLOW	0.455	0.455	0	0.4	0.4	0
OVERFLOW	0.307	0.327	5.86%	0.15	0.16	6.67%
UNDERFLOW	0.148	0.129	12.8%	0.25	0.24	4%

Fig.6 shows that grade efficiency and number of particle that exit from underflow of the hydrocyclone increased when greater particle is used.
After comparing CFD result with experimental result, be concluded that error in result is negligible.

4.1. Determination of Grade Efficiency h_G

To determine the Grade Efficiency, we injected 72 particles with specified diameter (35-125 micron) from inlet flow surface, and then the grade efficiency (h_G) was defined as follow:

$$h_G = \frac{Numerical\ of\ particles\ that\ exit\ from\ under\ flow}{72\ (\ total\ number\ of\ injected\ particles\ )} \times 100$$
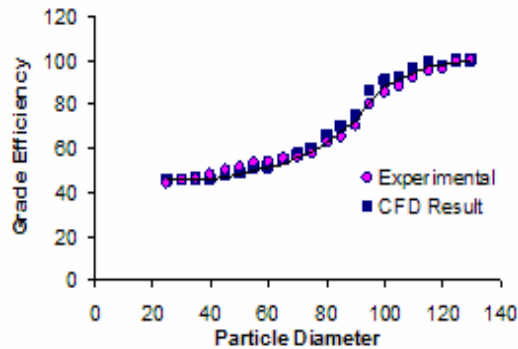

Fig. 6. Grade Efficiency V.S Particle Diameter

Table. 4. Grade Efficiency V.S Particle Diameters

Particle Diameter (micrometers)	No. of Particles in Under Flow	No. of Particles in Over Flow	Grade Efficiency
D=35	33	39	45.8333
D=40	33	39	45.8333
D=45	34	38	47.2222
D=50	35	37	48.6111
D=55	37	35	51.3889
D=60	37	35	51.3889
D=65	39	33	54.1667
D=70	41	31	56.9444
D=75	43	29	59.7222
D=80	47	25	65.2778
D=85	50	22	69.4444
D=90	54	18	75
D=95	62	10	86.1111
D=100	65	7	90.2778
D=105	66	6	91.6667
D=110	69	3	95.8333
D=115	71	1	98.6111
D=120	70	2	97.2222
D=125	72	0	100

5. Experimental Setup

A laboratory hydrocyclone with a specific geometry is show in Fig.2. A glassy body hydrocyclone were used for experimental purpose. The full setup consisting of a pump P, control valves V, mixing tank M and pressure gauge G shown in Fig.7. Abypass valve V2 is used to

A defined amount of solid particles were allowed to mix in the mixing tank. The mixture is allowed to enter the hydrocyclone by the help of pump P. The under flow and over flow consideration were measured by collecting samples at a certain period of time.
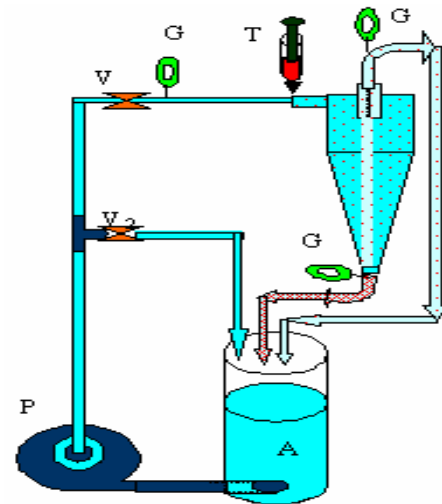
Fig. 7. Hydrocyclone Setup

6. Conclusion

A combination of increased available computational speed and advancements in software modeling has resulted in the capability to use CFD in modeling multiphase flows in hydro-cyclones. After comparing CFD result with experimental result, conclude that:

- In the injection process of particle with grater rotation radius, the separation phenomenon is possible in hydrocyclone.
- Wherever particles diameter is greater, the grade separation efficiency is also greater.

- The experimental result is a validation for numerical (CFD) result of this paper.

References

[1] Dahlstrom, D., 1949. *Cyclone operating factors and capacities on coal and refuse slurries*. Trans. Am. Inst. Min. Eng. 184,331– 344.

[2]Yoshiota, N., Hotta, Y., 1955. *Liquid cyclone as a hydraulic classifier.Chem*. Eng. Jpn. 19 (12), 632–640.

[3] Fahlstrom, P.H., 1963. Studies of the hydrocyclone as a classifier.In: Roberts, A. (Ed.), Proc. 6th Int. Miner. Process. Congr.,Cannes. Pergamon, London, pp. 87– 112.

[4] Agar, G.E., Herbst, J.A., 1966. *The effect of fluid viscosity on cyclone classification*. Soc. Min. Eng., 145–149 (June).

[5] Lynch, A.J., Rao, T.C., 1975. *Modeling and scale-up of hydrocyclone classifiers*. In: Carta, M. (Ed.), Proc. 11th Int. Miner.Process. Congr., Cagliari. Aziende Tipografiche Bardi, Rome,pp. 245– 269.

[6] Plitt, I.R., 1976. *A mathematical model of the hydrocyclone classifier.*CIM Bull., 114– 123.

[7] Bloor, M.I.G., Ingham, D.B., 1987. *The flow in industrial cyclones*. J. Fluid Mech. 178, 507–519.

[8] Kelsal, D.F., 1952. *A study of the motion of solid particles in a hydraulic cyclone. Trans*. Inst. Chem. Eng. 30, 87– 108.

[9] Hutchinson, B.R., Raithby, G.D., 1986. *A multigrid method based on the additive correction strategy*. Numer. Heat Transf. 9,511 –537.

[10] Pericleous, K.A., Rhodes, N., Cutting, G.W., 1984. *A mathematical model for predicting the flow field in a hydrocyclone classifier.Proc*. Int.Conf. Hydrocyclones. Bath, England, pp. 27–38.

[11] Hsieh, K.T., Rajamani, R.K., 1991. *A mathematical model of the hydrocyclone based on physics of fluid flow*. AIChE J. 37, 735– 746.

[12] Monredon, T.C, Hsieh, K.T., Rajamani, R.K., 1990. *Fluid flow model of the hydrocyclone: an investigation of device dimensions*. Int. J. Miner. Process. 35, 65–83.

[13] Boysan, F., Ayers, W.H, Swithenbank, J., 1982. *A fundamental mathematical modelling approach to cyclone design*. Trans. Ichem. E. 60, 222– 230.

[14] Davidson, M.R., 1988. *Numerical calculations of flow in a hydrocyclone operating without an air core*. Appl. Math. Model. 12, 119–128.

[15] Cristea, E.D, Malfa, E., Coghe, A., 1994. *3D simulation and experiments of cement rotary kiln preheater top cyclone. Fluent Users Group Meeting* UK.

[16] Mathur, S.R., Murthy, J.Y., 1997. *A pressure-based method for unstructured meshes. Numer.* Heat Transf., Part B Fundam. 31, 195– 215.

[17] Hoekstra, A.J., Derksen, J.J., Van den Akker, H.E.A., 1999. *An experimental and numerical study of turbulent swirling flow in gas cyclones*. Chem. Eng. Sci. 54, 2055–2065.

[18] Kuehlert, K. and Andrade. P., 2002. *Positioning of GAMBIT Application Specific Template*. Fluent Incorporated internal memo.

[19] Casey, M. and Wintergerste, T., 2000. *Quality and trust in Industrial CFD*. ERCOFTAC.

[20] Cokljat, D., Slack, M. and Vasquez, S., 2003. *Reynolds-Stress Model for Eulerian Multiphase.* submitted to Turbulence heat and Mass Transfer 4.
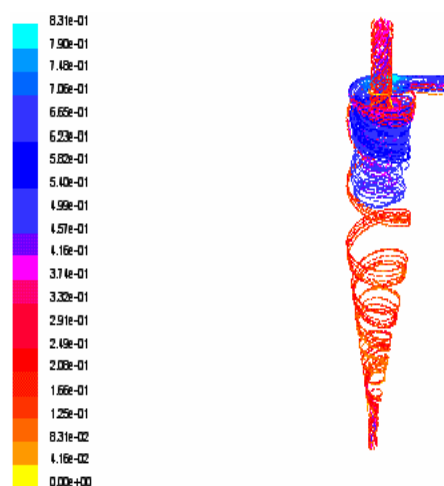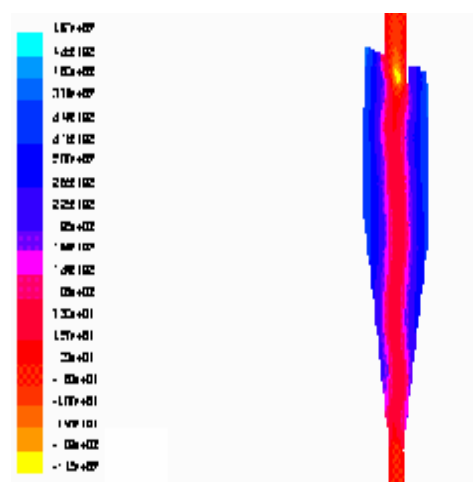
Fig. 8. Path Lines of Water

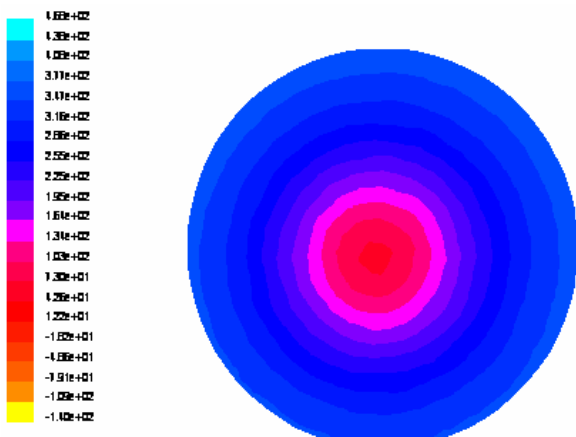**Fig. 9. Pressure in a Vertical Face for Liquid Phase**

Fig.10. Pressure in a Horizontal Face for Liquid Phase
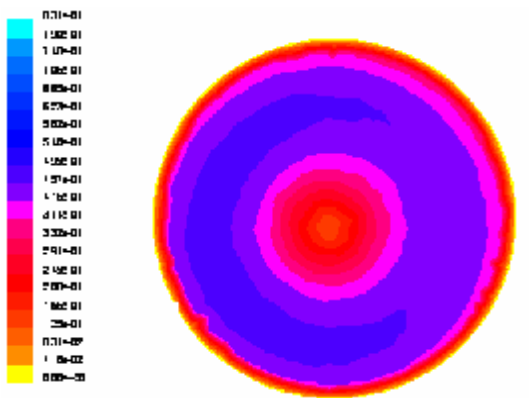

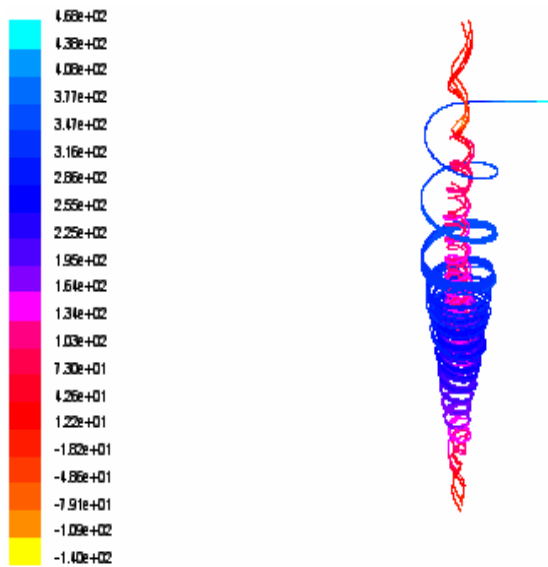**Fig. 11. Velocity in a Horizontal Face for Liquid Phase**

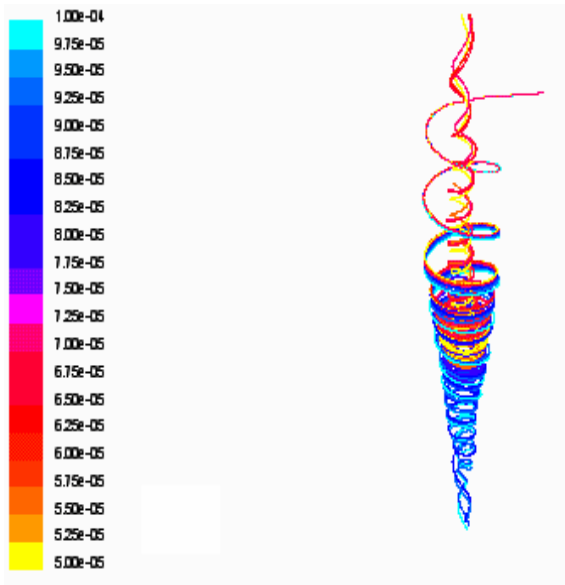**Fig. 12. Path Lines of Particle vs Total Press**

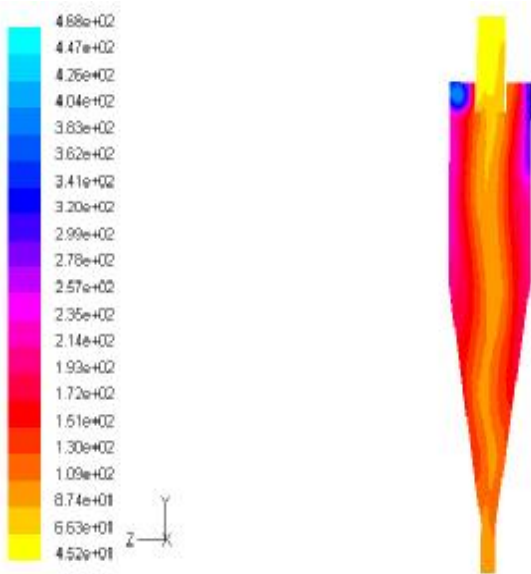**Fig. 13. Particle Size Distribution**

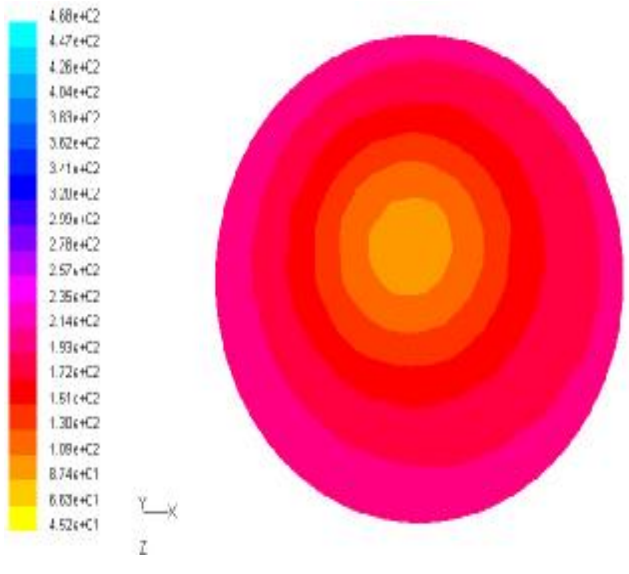**Fig. 14. Pressure in a vertical face for discrete phase**

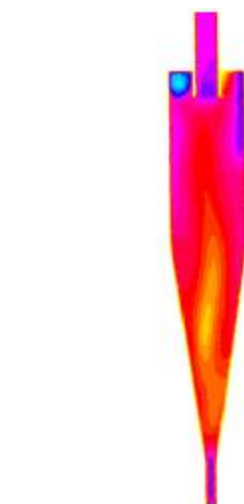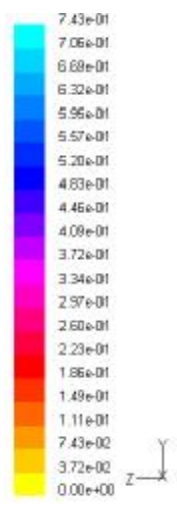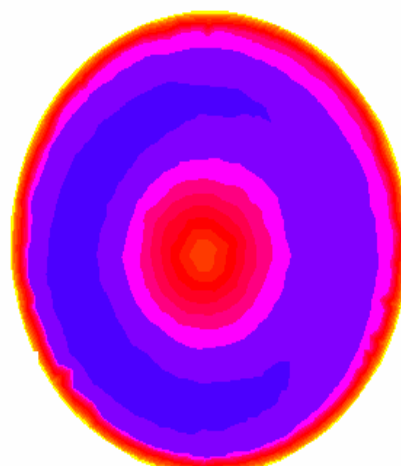**Fig. 15. Pressure in a horizontal face for discrete phase**

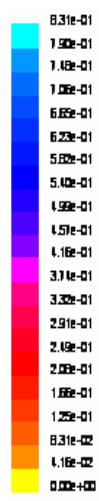**Fig. 16. Velocity in a Vertical Face for Discrete Phase**

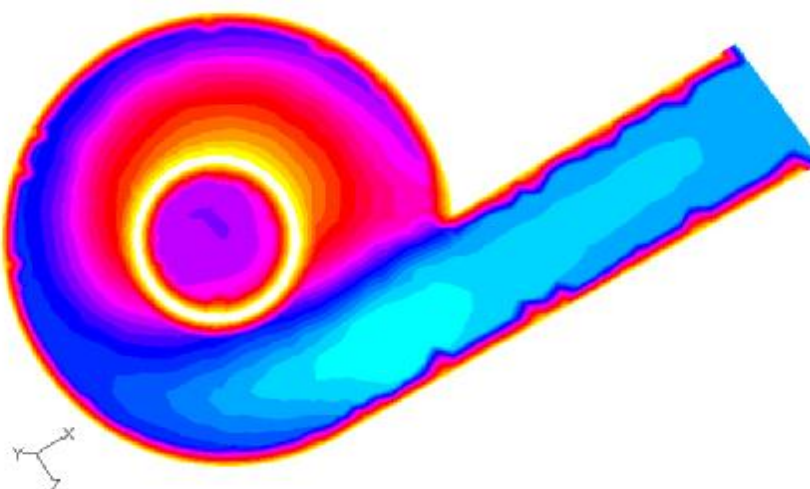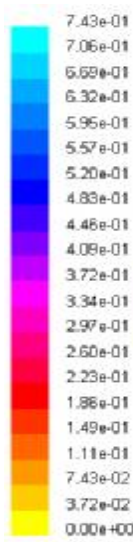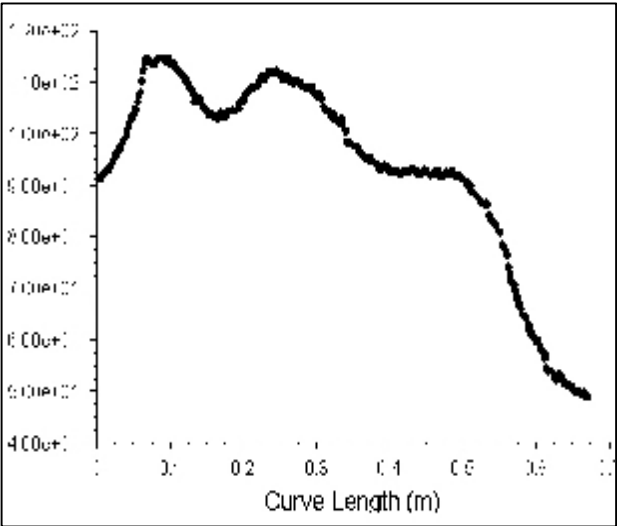**Fig. 17. Velocity in a Horizontal Face for Discrete Phase**
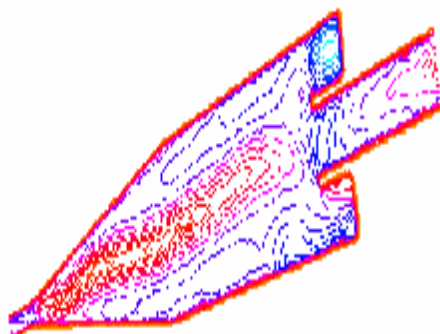
Fig. 18. Line Velocity in a Vertical Face for Discrete Phase

Fig. 19. Line Velocity in a Horizontal Face for Discrete Phase

Fig. 20. Velocity in a Horizontal Face From Top for Discrete Phase

Fig. 21. Total Pressure in a Vertical Face (Pa)
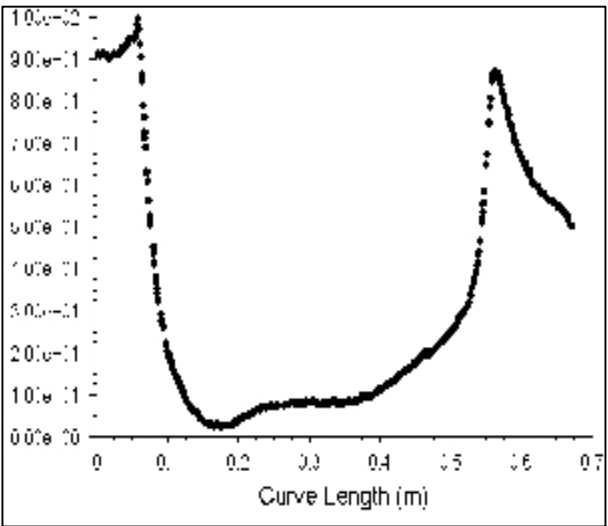
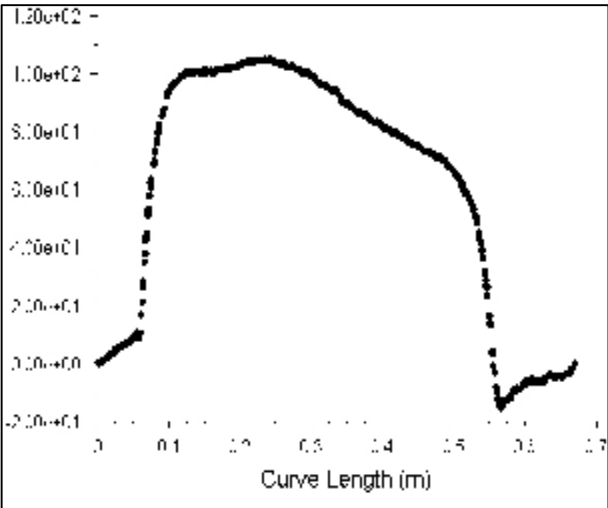**Fig. 22. Dynamic Ppressure in a Vertical Face (Pa)**
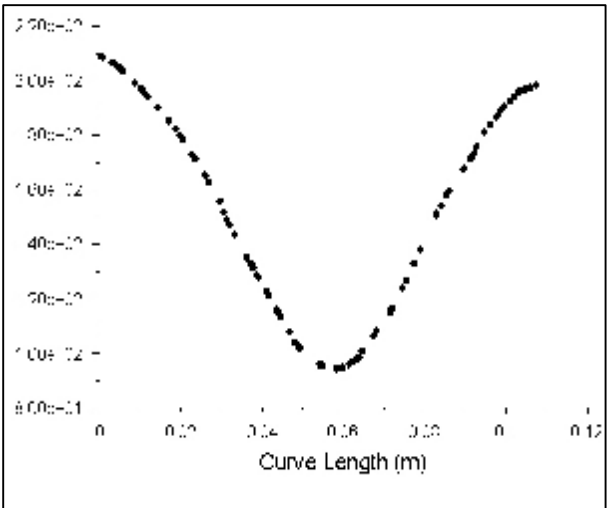

Fig. 23. Static Pressure in a Vertical Face (Pa)

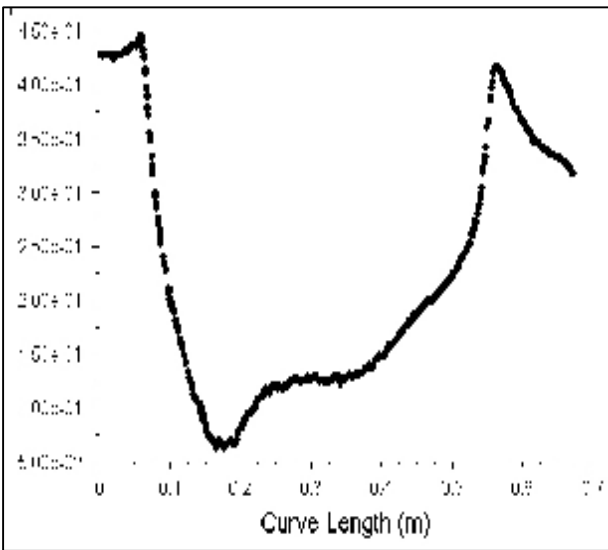**Fig. 24. Total Pressure in a Horizontal Face (Pa)**

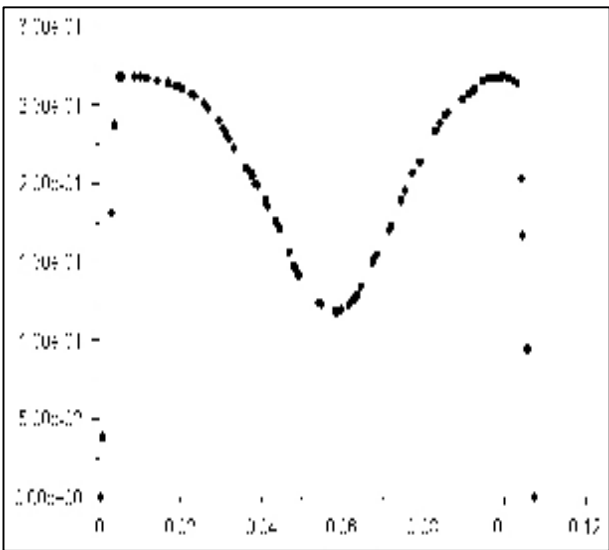**Fig. 25. Velocity Magnitude in a Horizontal Face (m/s)**

Fig. 26. Velocity Magnitude in a Vertical Face (m/s)
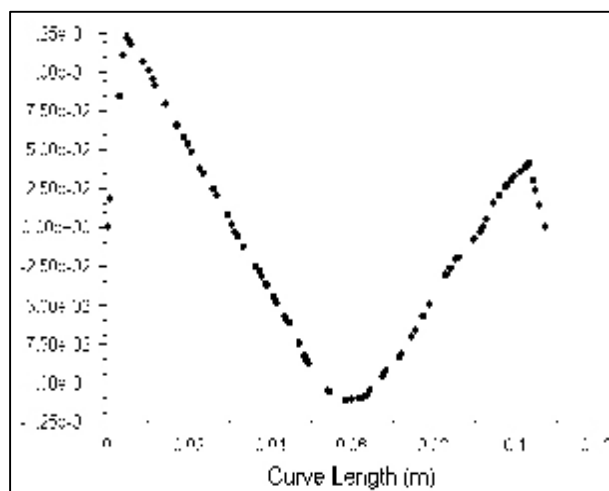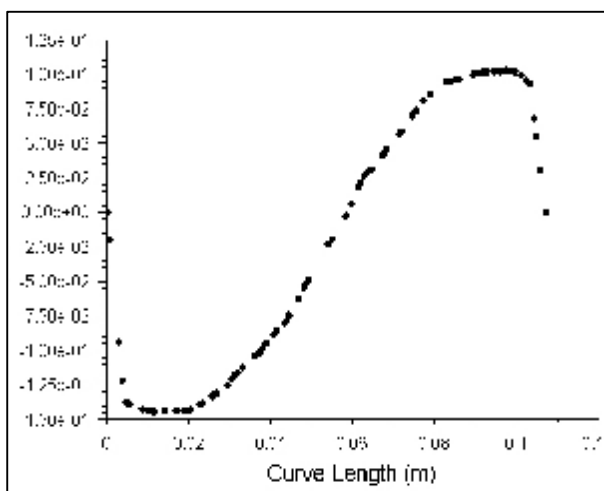
Fig. 27. Radial Velocity in a Horizontal Face (m/s)

Fig. 28. Axial Velocity in a Vertical Face (m/s)